Chemical Engineering Journal 316 (2017) 137–145

Contents lists available at ScienceDirect

Chemical Engineering Journal

journal homepage: www.elsevier.com/locate/cej

Rational design of Co_3O_4/Co/carbon nanocages composites from metal organic frameworks as an advanced lithium-ion battery anode

Kaiqiang Zhou [a,b], Lanfang Lai [a], Yichao Zhen [a], Zhensheng Hong [a,b,*], Juhua Guo [c], Zhigao Huang [a,b]

[a] College of Physics and Energy, Fujian Normal University, Fujian Provincial Key Laboratory of Quantum Manipulation and New Energy Materials, Fuzhou 350117, China
[b] Fujian Provincial Collaborative Innovation Center for Optoelectronic Semiconductors and Efficient Devices, Xiamen 361005, China
[c] College of Chemistry and Chemical Engineering, Fujian Normal University, Fuzhou, Fujian 350007, China

HIGHLIGHTS

- We design a composite material of Co_3O_4@Co@carbon nanocages (COCCNCs).
- COCCNCs possess a very large surface area and mesoporous structure.
- COCCNCs exhibited high Coulombic efficiency and superior rate capability for LIBs.
- A stable capacity of 505 mA hg^{-1} can be remained after 600 cycles at 2000 mA g^{-1}.

ARTICLE INFO

Article history:
Received 23 November 2016
Received in revised form 9 January 2017
Accepted 16 January 2017
Available online 17 January 2017

Keywords:
Co_3O_4
Metal organic frameworks
Carbon nanocages
Lithium ion batteries

ABSTRACT

In this paper, Co-based metal organic frameworks were prepared through a facile method. After successive carbonization and oxidation treatment, the Co_3O_4/Co/carbon nanocages (COCCNCs) with hollow dodecahedral shape were obtained. Co_3O_4/Co/carbon nanocages with a high surface area (183.9 m^2 g^{-1}) and uniform pore distribution were employed as an anode material for LIBs and exhibited a high reversible specific capacity (850 mA hg^{-1} at 100 mA g^{-1}), improved Coulombic efficiency, superior rate capability (485 mA hg^{-1} at a high current density of 5000 mA g^{-1}) and excellent cycling stability (505 mA hg^{-1} can be remained after 600 cycles at 2000 mA g^{-1}). Such a superior lithium storage performance is largely ascribed to the unique architecture composed of well-dispersed Co_3O_4 (ca. 9 nm) and Co (ca. 5 nm) nanocrystals embedded in hollow carbon nanocages with graphitic structure. This architecture not only avoids particle aggregation and nanostructure cracking upon cycling, but also provides continuous and flexile conductive carbon frameworks to facilitate the fast ions and electrons transportation.

1. Introduction

As one of the most promising energy storage devices, lithium ion batteries (LIBs) have been widely applied in different portable electronics [1]. Since LIBs were introduced into commercial electronic products by Sony [2], graphite has been used as the typical anode material. However, the theoretical capacity (372 mA hg^{-1}) and poor rate performance of graphite is far short of the demands for large scale applications like electrical and hybrid electrical vehicles (EVs and HEVs) [3–6], where higher energy density and power density are particularly important. A class of emerging anode materials, transition metal oxides (MO_x, M = Mn, Fe, Ni, Co, Sn, etc.) have attracted much attention due to their higher specific capacities [7–10]. However, there are several obstacles of those metal oxides to be used in LIBs [11–13]: (1) large volume change upon lithiation and delithiation; (2) poor electrical conductivity; (3) low coulombic efficiency. Therefore, various strategies have been carried out for solving those obstacles and enhancing the electrochemical performance. For instance, nanostructured materials, with high specific surface area and robust structure, can accommodate the volume expansion and shrinkage during insertion and extraction process of lithium ion [13–18]. Hybridization with conductive carbonaceous substrates (amorphous carbon, carbon nanotube and graphene) is a common approach to enhance the conductivity and electrochemical properties of the electrodes materials [19–24].

Recently, metal organic frameworks (MOFs) was used to prepare transition metal oxide nanostructures due to its high surface areas, large pore volumes and well defined pore size distributions

* Corresponding author at: College of Physics and Energy, Fujian Normal University, Fujian Provincial Key Laboratory of Quantum Manipulation and New Energy Materials, Fuzhou 350117, China.
E-mail address: winter0514@163.com (Z. Hong).

http://dx.doi.org/10.1016/j.cej.2017.01.060
1385-8947/

[25]. Through thermal annealing MOFs materials, carbon-coated transition metal oxide with desired structure can be obtained in a facile process [26–30]. For distance, Zou et al. reported hierarchical yolk-shell NiO/Ni/Graphene nanostructures derived from Ni-based MOF [26], which exhibited nearly no capacity loss for Li-ion storage after 1000 cycles. It was demonstrated that mixed valence metal oxides hollow structures (CuO/Cu_2O) were successfully prepared from MOFs, which could provide superior performance as anode materials in LIBs (740 mA hg^{-1} at 100 mA g^{-1}) [27]. A porous carbon electrode with embedded ZnO quantum dots was prepared by annealing Zn-based MOFs, reaching a reversible capacity of 1200 mA hg^{-1} [28]. Other metal oxides or sulfides such as Fe_2O_3, TiO_2, CoS and NiS derived from MOFs were also reported and show promising applications as anode materials in LIBs [31–34]. These studies inspire us to design anode materials derived from MOFs with enhanced Li-ion.

In this work, Co_3O_4/Co/carbon nanocages (COCCNCs) with hollow polyhedral shape were synthesized through two steps of thermal annealing of Co-based MOFs (ZIF-67). Such composites with rational design have a high surface area and porous structure, robust carbon framework and hollow structure, which can provide a well-contact between electrode and electrolyte and more active sites, possess a good conductive network and structural stability of the electrode. Therefore, COCCNCs was used as anode electrode for LIBs and exhibited a high reversible capacity, improved Coulombic efficiency, superior rate capability and excellent cycling stability.

2. Experimental

2.1. Materials synthesis

Co_3O_4/Co/carbon nanocages (COCCNCs) were synthesized by using Co-based metal organic frameworks as a precursor. The Co-based MOF (ZIF-67) was synthesized according to previous report with minor modifications [34]. Typically, 0.45 g $Co(NO_3)_2{\cdot}6H_2O$ were dissolved in 5 mL deionized water to form solution A. 5.5 g 2-Methylimidazole was dissolved in 20 mL deionized water to form solution B. Then, the solution A was poured into solution B slowly and stirred for 6 h at room temperature. The resulting purple precipitate was collected by centrifugation, washed with alcohol and deionized water for several times and dried at 60 °C for 12 h. Subsequently, as-prepared ZIF-67 precursors were put into tube furnace with an Ar flow and calcined at 400 °C for 2 h and then raised to 600 °C for 3 h with a rate of 1 °Cmin^{-1}. The black powders (Co/carbon nanocages, named CCNCs) were obtained. In order to obtain COCCNCs, the second thermal treatment was carried out. Directly, CCNCs were heated at 220 °C for 1.5 h in air with a rate of 0.5 °Cmin^{-1}. As a reference, pure Co_3O_4 sample was obtained when the calcination time was continued for 4 h in air.

2.2. Characterizations of the samples

X-ray diffraction (XRD) patterns were recorded on a Rigaku Ultima IV diffractometer, using Cu Kα radiation (λ = 1.5406 Å). Scanning electron microscopy (SEM, S8010 instrument), coupled to energy dispersive X-ray analysis (EDX) and transmission electron microscopy (TEM, FEI F20 S-TWIN instrument) were performed for the morphological and structural characterization of the obtained samples. N_2 adsorption-desorption analysis was measured on a Micro-meritics Tristar II 3020 instrument (USA). The pore size distributions of the as-prepared samples were analyzed using the Barrett Joyner Halenda (BJH) method. The surface electronic state of material was characterized by Thermo Scientific Escalab 250Xi.

2.3. Electrochemical measurements

The active materials dried at 120 °C for 12 h in a vacuum oven were admixed with super-P (SCM Industrial Chemical Co. Ltd.)

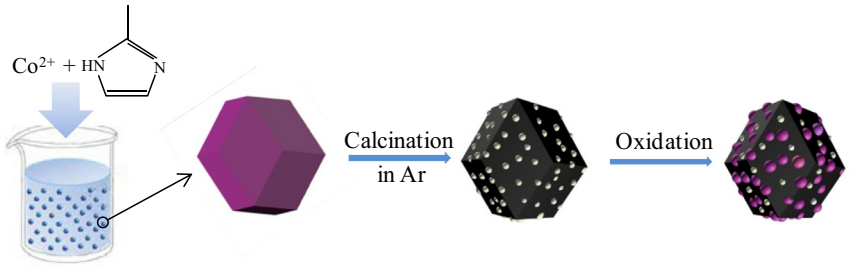

Fig. 1. Schematic illustration of the formation of COCCNCs composites.

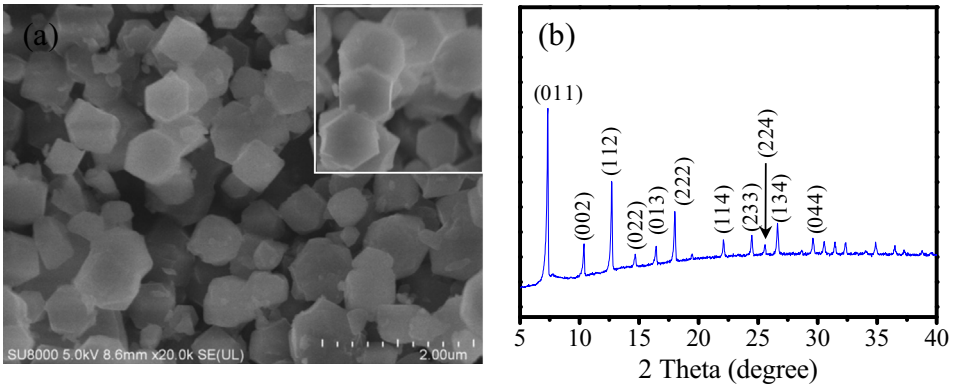

Fig. 2. SEM image (a) and XRD pattern (b) of ZIF-67.

and polyvinylidene fluoride (PVDF, SCM) binder additive in a weight ratio of 70:15:15. The mixture was spread and pressed on circular copper foils as working electrodes (WE), and dried at 120 °C in vacuum for 12 h. The mass loading of active material in the electrode was around 1.2 mg cm^{-2}. The coin cells were assembled in an argon-filled glove box, in which the concentration of water and oxygen was kept below 1 ppm. Cyclic voltammetry (CV) measurements were performed on Zennium (Zahner). The galvanostatic charge/discharge measurements of the cells were carried out by a multichannel battery testing system (Wuhan, LAND, China) with a potential window ranging from 0.01 to 3.0 V at various current densities. Cyclic voltammograms (CV) measurements at a scanning rate of 0.5 mV S^{-1} were performed by Arbin instruments (BT-2000). Electrochemical impedance spectroscopy (EIS) was also conducted on Zennium electrochemical workstation with an AC voltage amplitude of 5 mV in the frequency range from 1 MHz to 100 mHz.

3. Results and discussion

Co_3O_4/Co/carbon nanocages (COCCNCs) were fabricated based on the scheme illustrated in Fig. 1. Firstly, Co-based metal organic frameworks (ZIF-67) were prepared from $Co(NO_3)_2{\cdot}6H_2O$ and 2-Methylimidazole in deion water with a vividly stir under a room-temperature condition. Secondly, Co/carbon nanocages (CCNCs) were obtained after heat treatment of ZIF-67 precursors under Ar condition. Finally, COCCNCs were prepared after oxidation treatment of CCNCs at Air atmosphere.

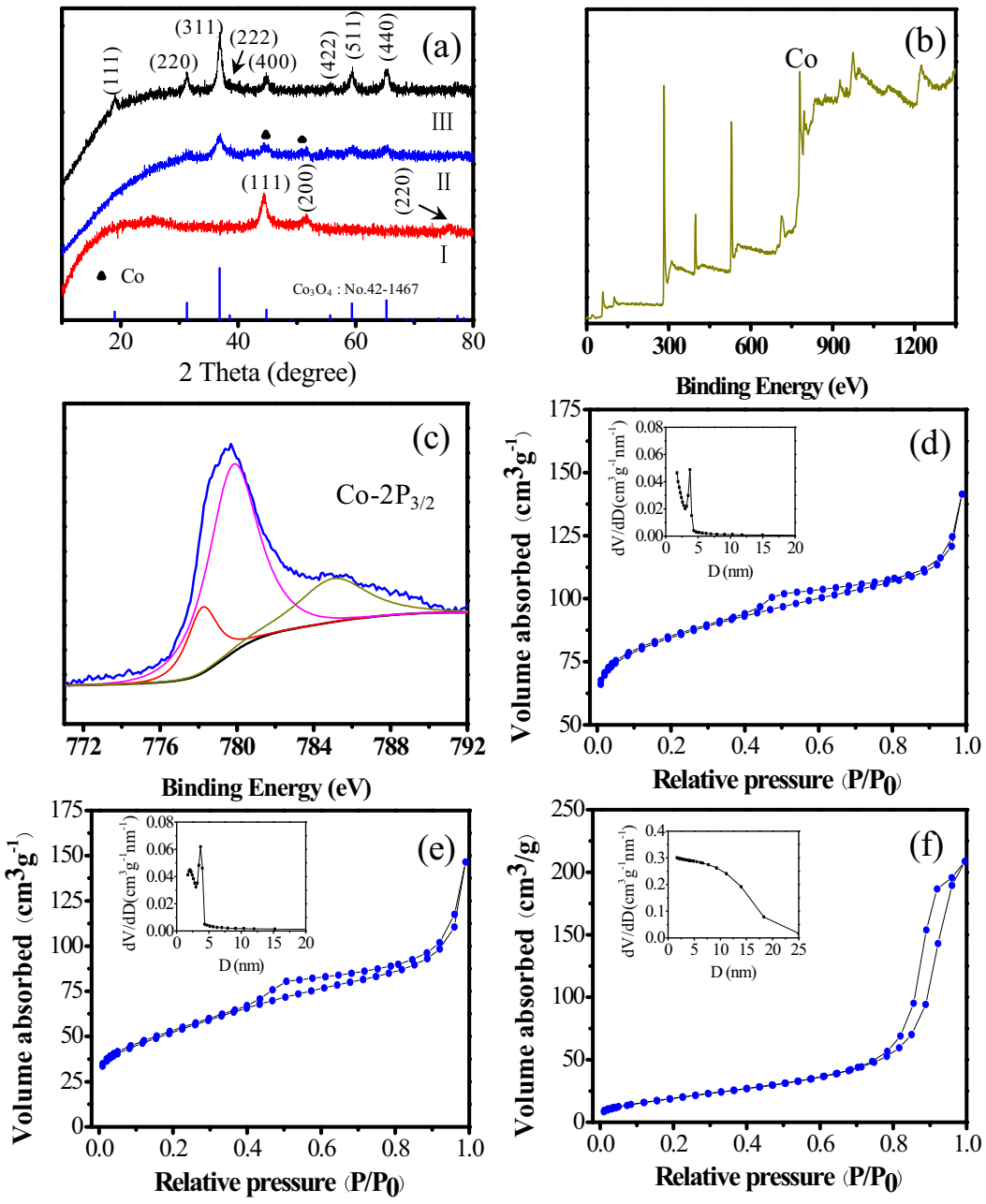

Fig. 3. (a) XRD patterns of CCNCs (I), COCCNCs (II) and Co_3O_4 (III). XPS spectra of COCNCs: (b) full spectrum, (c) Co-$2P_{3/2}$. Nitrogen adsorption-desorption isotherms of COCCNCs (d), CCNCs (e) and Co_3O_4 (f), the insets of (d), (e) and (f) are the corresponding BJH pore size distribution.

Fig. 2a shows the SEM image of ZIF-67, such sample has a polyhedral shape with size of 700–900 nm. The typical XRD pattern of ZIF-67 is shown in Fig. 2b. All the peaks show excellent consistency with the previous report [35]. Fig. 3a shows XRD patterns of the samples after thermal annealing. In the curve I, the peaks of ZIF-67 disappear and three peaks at 44.2°, 51.5° and 75.8° are clearly observed. This demonstrates the cobalt metal was obtained after the first thermal treatment at an Ar atmosphere, which can be well identified according to JCPDS card No. 15-0806. The curve II shows the sample annealed at 220 °C for 1.5 h in air, whose phases include Co_3O_4 (JCPDS No. 42-1467) and cobalt metal. This result verifies the oxidation of cobalt metal to cobalt oxide. The XRD pattern of the sample after complete oxidation is displayed in curve III, which demonstrates the pure phase of Co_3O_4 (JCPDS No. 42-1467). The broadened diffraction peaks of COCCNCs suggest a small crystallite size. The sharper diffraction peaks of Co_3O_4 indicate a higher crystallite size. In order to investigate the state of cobalt element, XPS spectra were carried out and the data was shown in Fig. 3b, c. Fig. 3b shows the full spectrum and the cobalt element can be observed around 780 eV. The Co $2p_{3/2}$ spectrum was shown in Fig. 3c. The small peak at 778.2 eV demonstrates the presence of cobalt metal and the main peak around 779.8 eV is ascribed to Co^{3+} and Co^{2+} from Co_3O_4 phase, indicating the existence of Co and Co_3O_4 in COCCNCs [36].

N_2 adsorption-desorption isotherms measurements were adopted to investigate the Brunauer-Emmett-Teller (BET) surface area and pore size distribution, as shown in Fig. 3d–f. The surface area of Co@carbon nanocages (CCNCs) is up to 279.4 $m^2 g^{-1}$, which is largest among the three samples. The value of COCCNCs and Co_3O_4 is 183.9 $m^2 g^{-1}$ and 72.5 $m^2 g^{-1}$, respectively. CCNCs (inset in Fig. 3d) show a uniform pore distribution with size around 3.7 nm, suggesting that the as-prepared carbon nanocages have a fine mesoporous structure. COCCNCs (inset in Fig. 3e) basically have a similar pore size distribution with that of CCNCs, which

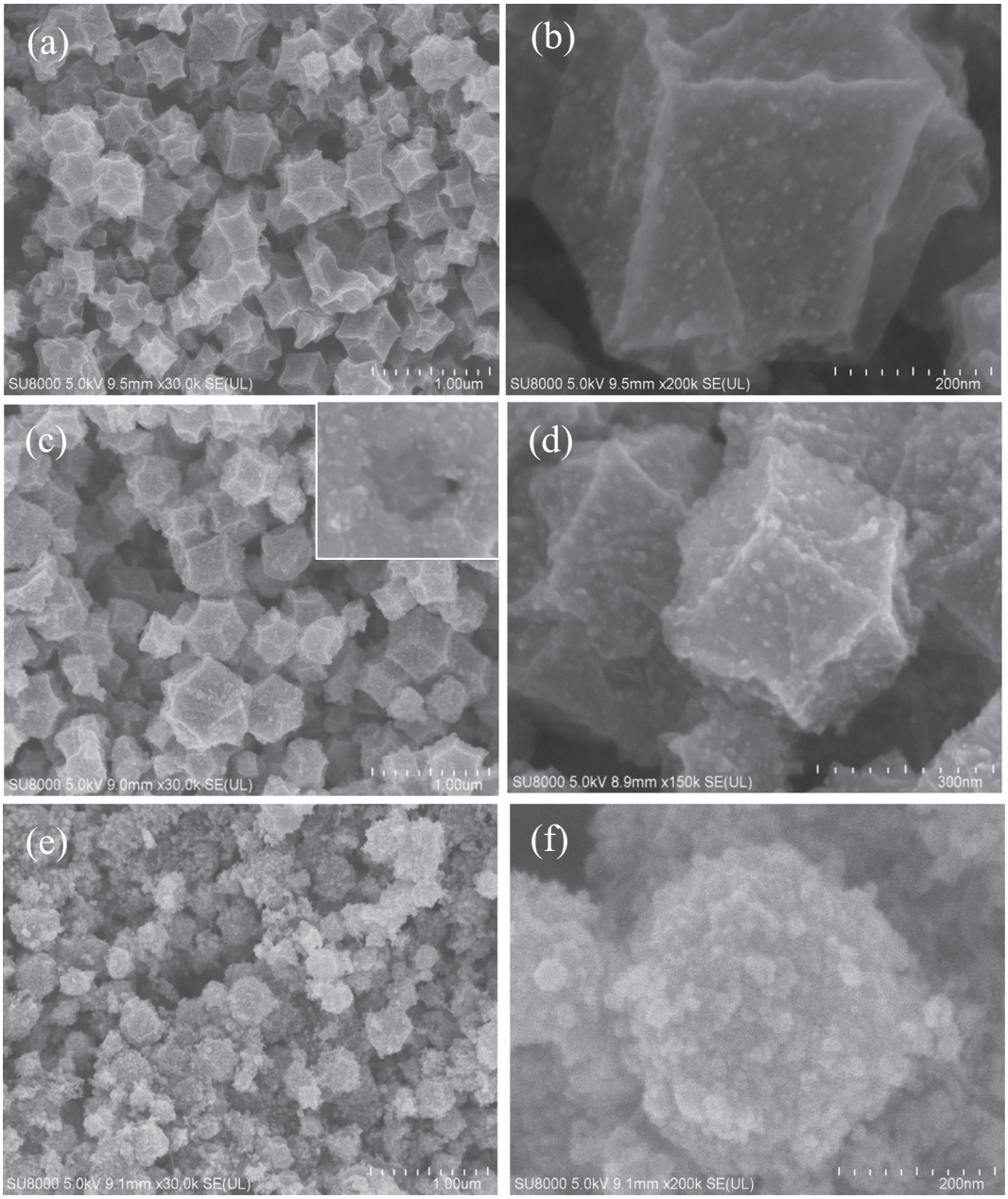

Fig. 4. SEM images of CCNCs (a, b), COCCNCs (b, c) and Co_3O_4 (e, f), the inset image in (c) is a magnification SEM image of COCCNCs.

indicating that the mesoporous structure of carbon nanocages can be retained. However, the uniform mesopore distribution was broken after complete oxidation treatment, as shown in Fig. 3f (inset). This could be understood that the framework of carbon nanocages would be destroyed after thermal annealing under air condition, which would be discussed at the next section. It has been demonstrated that large surface area and uniform pore size distribution can facilitate well contacts between electrode-electrolyte as well as the Li^+ diffusion and intercalation [37]. Therefore, these results suggest COCCNCs and CCNCs could be expected with much better electrochemical performance in LIBs.

The morphology and structure of the as-prepared samples were investigated using scanning electron microscopy (SEM) and transmission electron microscopy (TEM). As shown in the Fig. 4a, b, the carbon nanocages (CCNCs) with size of 200–400 nm are clearly observed and many cobalt nanoparticles homogeneously spread on the carbon frameworks. Compared with CCNCs, the framework of carbon nanocages can be retained in COCCNCs and the size of a part of nanoparticles become little bigger because the cobalt metal nanoparticles convert to Co_3O_4 nanoparticles (Fig. 4c, d). The inset in Fig. 4c illustrates that the carbon nanocages have a hollow structure. From the high-magnification SEM images (Fig. 4b and Fig. 4d), it can be observed the carbon nanocages can effectively prevent the aggregation and growth of cobalt and cobalt oxide nanoparticles, even during the oxidation process of cobalt nanoparticles. However, since the second thermal treatment was prolonged to 4 h, the hollow carbon architecture was destroyed and Co_3O_4 balls were observed, as shown in the Fig. 4e, f. Co_3O_4 balls are constructed by numerous nanoparticles. From the SEM images of three samples, the size of Co_3O_4 nanoparticles is the biggest than others, which is consistent with the XRD results. This is due to the growth or aggregation of Co_3O_4 nanoparticles after the breakage of the framework of carbon nanocages.

TEM and HRTEM images of COCCNCs were presented in Fig. 5a and b. Hollow structural polyhedral could further be observed from the TEM image. It also can be seen that nanodots with the size of ca. 5 nm for Co metal and ca. 9 nm for Co_3O_4 are well dispersed in the carbon framework. The lattice parameters are 0.25 nm for Co (1 1 0) and 0.29 nm for Co_3O_4 (2 2 0), respectively. Meanwhile, the carbon layer with a preferable crystallinity is presented in the Fig. 5b, suggesting the formation of graphitic carbon. It's demonstrated that such graphitic carbon derived from metal organic frameworks possesses good conductivity [38]. The SEM image and elemental mapping images of COCCNCs are shown in Fig. 5c. Several elements such as Co, C, N and O are uniformly distributed in the polyhedral. The EDX results indicate that the elements contents of Co, C, N and O are about 14.4%, 62.8%, 7.7% and 15.1%, the elements mass contents of Co, C, N and O are about 43.5%, 38.6%, 5.52% and 12.38%.

In order to test the electrochemical performance of as-prepared samples, cyclic voltammetry (CV) was separately conducted at a scan rate of 0.5 mV s^{-1} in the voltage range of 0.01–3 V. Fig. 6a shows the CV curves of COCCNCs. A broad cathodic peak around 0.5 V in the first discharge can be attributed to the conversion reactions and the formation of solid electrolyte interface (SEI), similar result was also found for CCNCs (Fig. 6c). A small peak around 1.72 V may be attributed to lithium ion insertion to nitrogen-doped carbon materials [38]. The broad anodic peaks around 1.28 V and 2.17 V in the first charge are ascribed to the oxidation reactions of metallic cobalt [39–42]. However, Co_3O_4 electrode (Fig. 6e) shows some different results from COCCNCs and CCNCs. A peak shift from 0.5 V to 0.6 V at initial cathodic scan in pure

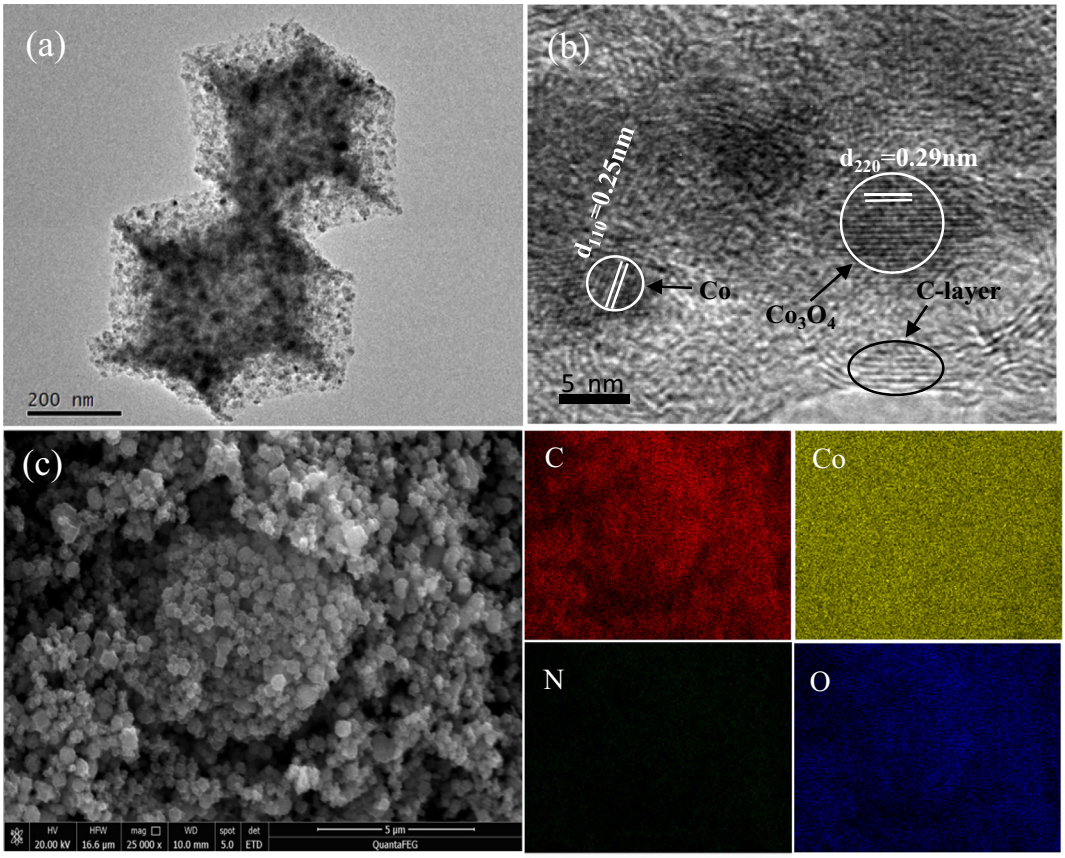

Fig. 5. TEM and HRTEM images of COCCNCs (a, b), SEM image of COCCNCs and C, Co, N and O element mapping images of COCCNCs.

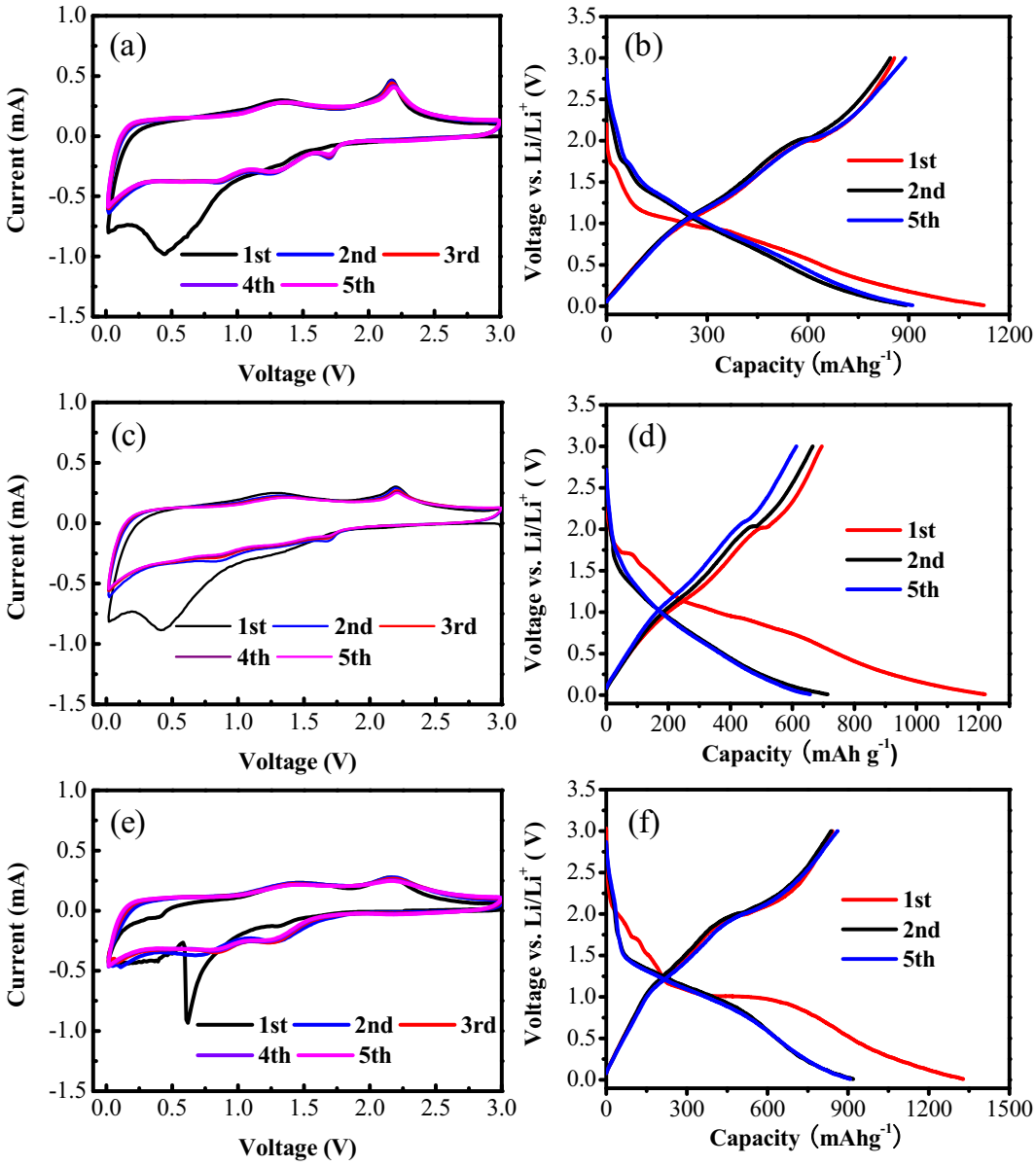

Fig. 6. Consecutive CV curves of COCCNCs (a), CCNCs (c) and Co_3O_4 (e) at a scan rate of 0.5 mV s^{-1} in the voltage range of 0.01–3 V. Discharge and charge profiles for the 1st, 2 nd and 5 th cycles of COCCNCs (b) CCNCs (d) and Co_3O_4 (f).

Co_3O_4 is observed, which is described as the typical CV curve of Co_3O_4 electrode [43]. The charge-discharge profiles of as-prepared samples at 100 mAg^{-1} in the potential window of 0.01–3.0 V are presented in the Fig. 6b, d, f. COCCNCs exhibit a discharge capacity of 1158 mA hg^{-1} (1221 mA hg^{-1} for CCNCs, 1328 mA hg^{-1} for Co_3O_4) and charge capacity of 867 mA hg^{-1} (695 mA hg^{-1} for CCNCs, 841 mA hg^{-1} for Co_3O_4). Therefore, the reversible capacity of COCCNCs is largest and it exhibited much improved Coulombic efficiency of 75% at the first cycle, which is higher than that of CCNCs (53%) and Co_3O_4 (62%). Although CCNCs and Co_3O_4 display a little larger first discharge capacity, the large irreversible capacities are not favor for the application in LIB. It should be noted that the first Coulombic efficiency of COCCNCs (75%) is much higher than that of Co_3O_4 nanorods coated by TiO_2 and porous graphene/Co_3O_4 cubes [13,17].

Fig. 7a shows the rate capability of COCCNCs (blue), CCNCs (red) and Co_3O_4 (black) electrodes at various current densities. At small current density of 100 mA g^{-1} and 200 mA g^{-1}, the stable charge capacity of COCCNCs is about 874 mA hg^{-1} (679 mA hg^{-1} for CCNCs, 851 mA hg^{-1} for Co_3O_4) and 842 mA hg^{-1} (552 mA hg^{-1} for CCNCs, 825 mA hg^{-1} for Co_3O_4). The reversible capacities of COCCNCs and Co_3O_4 are comparative, but both of them have larger capacity than that of CCNCs. At the current density of 1000, 2000, 5000 mA g^{-1}, COCCNCs exhibit stable capacity of 680, 585, 486 mA hg^{-1}, which are much larger than that of CCNCs and Co_3O_4. Particularly, the capacities of Co_3O_4 and CCNCs quickly dropped to 207 mA hg^{-1} and 152 mA hg^{-1} at 5000 mA g^{-1}. When the current density returned to 100 mA g^{-1}, the reversible capacity of COCCNCs can revert to 899 mA hg^{-1}, which is only 500 mA hg^{-1} for CCNCs and 625 mA hg^{-1} for Co_3O_4. Thus, COCCNCs demonstrated much enhanced Li-ion storage and electrochemical kinetics performance. These results can largely due to the synergistic effect of the unique architecture composed of well-dispersed Co_3O_4 nanocrystals embedded in hollow carbon nanocages with graphitic structure. The Co_3O_4 nanocrystals offer a large Li-ion storage capacity and carbon nanocages provides continuous and flexile

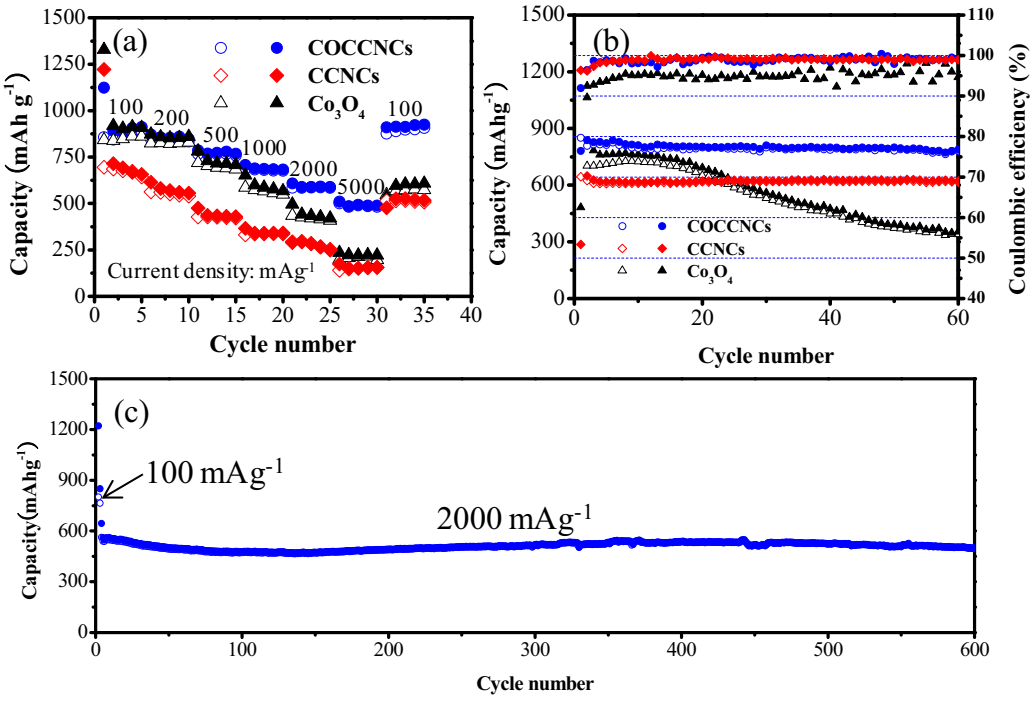

Fig. 7. (a) Rate capability for COCCNCs, CCNCs and Co_3O_4 electrodes at various current densities, (b) cycling performance and Coulombic efficiency of as-prepared samples (COCCNCs, CCNCs, Co_3O_4) at the current density of 100 mA g^{-1}, and (c) long cycling performance of COCCNCs electrode at a high current density of 2000 mA g^{-1}.

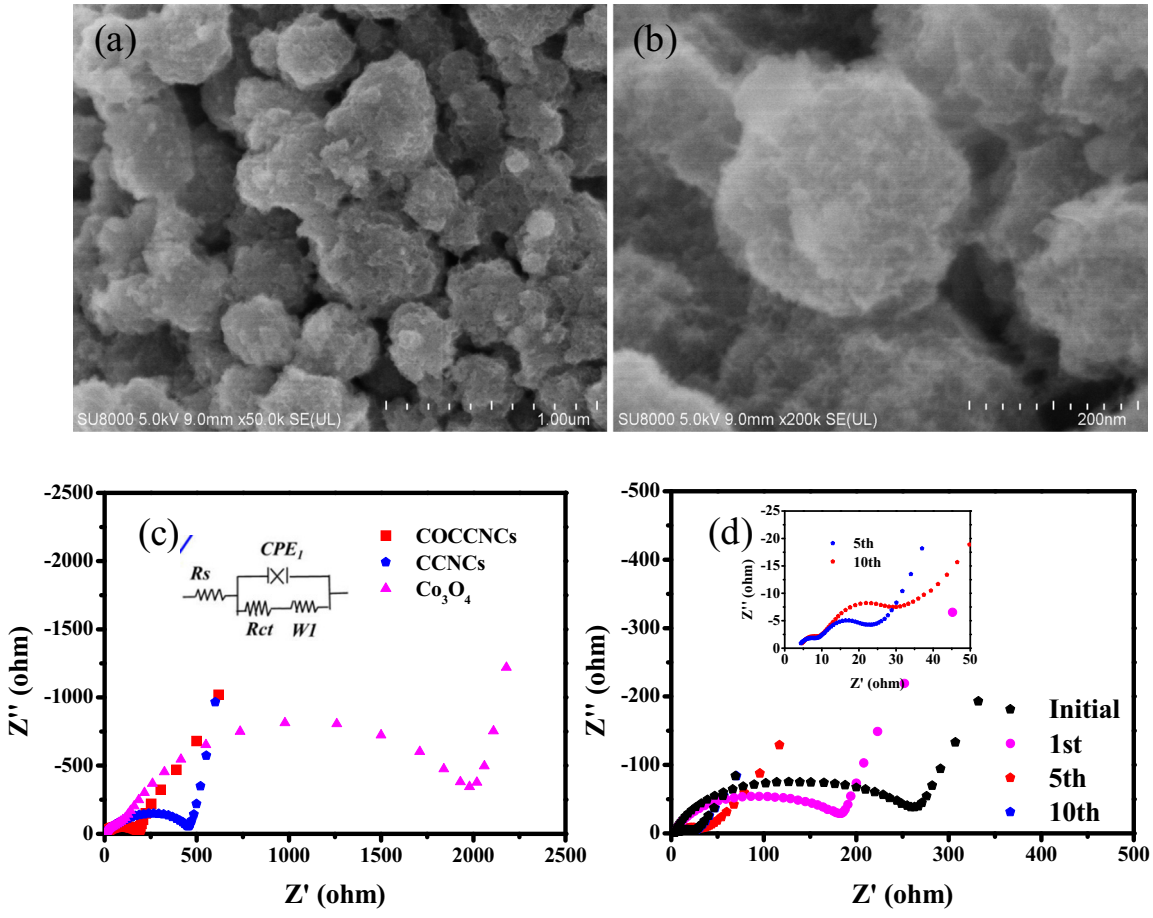

Fig. 8. (a and b) SEM images of COCCNCs after 600 charge-discharge cycles at current density of 2000 mA g^{-1}, electrochemical impedance spectra (EIS) of (c) the fresh batteries made of the three samples (COCCNCs, CCNCs and Co_3O_4) and (d) COCCNCs electrode after cycling tests. The inset in (c) is the corresponding equivalent circuit.

conductive carbon frameworks which facilitate the fast ions and electrons transportation. The unique architecture of COCCNCs tactfully combines the advantages from Co_3O_4 with high capacity and CCNCs with superior cycling stability. The disadvantages of CCNCs and Co_3O_4 can also be overcome in COCCNCs. Therefore, COCCNCs exhibits best lithium storage performance.

The cycling performance of the as-prepared samples at a constant current density of 100 mA g^{-1} is presented in Fig. 7b. It can be observed that the cycling stability of the Co_3O_4 is poor and the capacity less than 337 mA hg^{-1} was remained after 60 cycles. On the contrary, the capacity of COCCNCs (801 mA hg^{-1}) and CNCs (624 mA hg^{-1}) can be retained after 60 cycles, suggesting much better cycling stability. In addition, both of COCCNCs and CCNCs display a high Coulombic efficiency (near 99% after 5 cycles), which is only around 95% for Co_3O_4 at the same condition. Thus, COCCNCs inherit the large theoretical capacity from Co_3O_4 and good cycling stability from CCNCs, leading to a high performance anode material for LIBs. Meanwhile, COCCNCs electrode was tested at a high current density of 2000 mA g^{-1}. It demonstrated outstanding cycling performance with a capacity of 505 mA hg^{-1} after 600 cycles, which is larger than the other Co_3O_4 hybrid anodes [13,17]. The capacity retention can reach 90% (based on the first charge capacity) after 600 cycles. The superior lithium storage performance of COCCNCs can be attributed to the rationally designed structure including well-dispersed Co_3O_4 and Co tiny nanocrystals embedded in hollow N-doped carbon nanocages with graphitic structure. This architecture may not only avoid particle aggregation and nanostructure cracking upon cycling, but also provide continuous and flexile conductive carbon frameworks to facilitate the fast ions and electrons transportation.

In order to open out the reason of enhanced Li-ion storage properties for COCCNCs, the electrode over 600 cycles was characterized by SEM image. From Fig. 8a and b, a large number of active materials coated with SEI layers can be observed, the overall structure and morphology of COCCNCs electrode can be maintained after durative Li^+ insertion and extraction process. This stable structure is strongly favorable of avoid particle aggregation and nanostructure cracking upon cycling for conversion-type mechanism anode materials [27]. The AC impedance measurements have been carried out to investigate the electronic conduction as well as transfer processes of the electrode materials. Fig. 8c shows the electrochemical impedance spectroscopy (EIS) of COCCNCs, CCNCs and Co_3O_4. Each Nyquist plot comprises the electrolyte resistance (Rs) at high frequencies, a depressed semicircle at the middle frequencies arising from charge transfer resistance (Rct) and a slope at low frequencies representing the Warburg impedance (W) related to the diffusion process. Obviously, the Rct of CCNCs (457 Ω) was lower than that of Co_3O_4 (1897 Ω), but the Rct of COCCNCs composite electrode (257 Ω) is lowest among the three electrodes. The EIS results from the fresh cells made of COCCNCs and after cycling test (1, 10, 50 cycles at 0.1 Ag^{-1}) are also shown in Fig. 8d. It shows that the Rct of COCCNCs reduces with the increasing charge-discharge cycles, which had been reported in the previous papers [43,44]. This result can be attributed to the activation or the improved infiltrates of electrolyte into porous electrode material [45]. Therefore, it is verified that COCCNCs composite electrode has the best electronic conductivity. In short, the carbon nanocages can well maintain the structure and morphology of COCCNCs electrode, as well as enhanced electronic and ionic transportation, leading to an advanced lithium-ion battery anode.

4. Conclusion

In summary, the Co_3O_4/Co/carbon nanocages (COCCNCs) were successfully synthesized from cobalt based metal organic frameworks precursors, which were prepared through a facile method. Such composite material is composed of the N-doped carbon nanocages with graphitic structure and well-dispersed Co_3O_4 and Co tiny nanoparticles embedded in the nanocage matrix. COCCNCs also own a large specific surface area and uniform pore size distribution. When COCCNCs was employed as anode in LIBs, it exhibited improved Coulombic efficiency, superior rate capability and excellent cycling stability (505 mA hg^{-1} can be remained after 600 cycles at 2000 mA g^{-1}). This architecture can not only avoid particle aggregation and nanostructure cracking upon cycling, but also provides continuous and flexile conductive carbon frameworks for fast ions and electrons transportation. Thus, this research indicates that MOFs can be used as ideal precursors to fabricate metal oxides/carbon composite electrode materials with high performance through rational design.

Acknowledgements

This work was financially supported by National Natural Science Foundation of China (NSFC 51502038, 21406035 and U1505241), Research Fund for the Doctoral Program of Higher Education of China (RFDP 20133514110002), Natural Science Foundation of Fujian Province (2015J01042), and Education Department of Fujian Province (JA14081 and JA14076).

References

[1] J.M. Tarascon, M. Armand, Nature 414 (2001) 359–367.
[2] B. Dunn, H. Kamath, J.M. Tarascon, Science 334 (2011) 928–935.
[3] B. Scrosati, Nature 373 (1995) 557.
[4] D. Gu, W. Li, F. Wang, H. Bongard, B. Spliethoff, W. Schmidt, C. Weidenthaler, Y. Xia, D. Zhao, F. Schüth, Angew. Chem. Int. Ed. 54 (2015) 7060–7064.
[5] H. Geng, H. Ming, D. Ge, J. Zheng, H. Gu, Electrochim. Acta 157 (2015) 1–7.
[6] Y. Zhong, X. Xia, F. Shi, J. Zhan, J. Tu, H.J. Fan, Adv. Sci. 3 (2016) 1500286.
[7] K. Cao, L. Jiao, H. Liu, Y. Liu, Y. Wang, Z. Guo, H. Yuan, Adv. Energy Mater. 5 (2015) 1401421.
[8] X.L. Sun, C.L. Yan, Y. Chen, W.P. Si, J.W. Deng, S. Oswald, L.F. Liu, O.G. Schmidt, Adv. Energy Mater. 4 (2014) 1300912.
[9] L. Zhang, H.B. Wu, B. Liu, X.W. Lou, Energy Environ. Sci. 7 (2014) 1013–1017.
[10] H. Geng, Q. Zhou, Y. Pan, H. Gu, J. Zheng, Nanoscale 6 (2014) 3889–3894.
[11] M.V. Reddy, G.V. Subba Rao, B.V. Chowdari, Chem. Rev. 113 (2013) 5364–5457.
[12] J. Jiang, Y.Y. Li, J.P. Liu, X.T. Huang, C.Z. Yuan, X.W. Lou, Adv. Mater. 24 (2012) 5166–5180.
[13] H. Geng, Y. Guo, X. Ding, H. Wang, Y. Zhang, X. Wu, J. Jiang, J. Zheng, Y. Yang, H. Gu, Nanoscale 8 (2016) 7688–7694.
[14] Y. Kim, J.H. Lee, S. Cho, Y. Kwon, I. In, J. Lee, N.H. You, E. Reichmanis, H. Ko, K.T. Lee, ACS Nano 8 (2014) 6701–6712.
[15] Z.S. Hong, K.Q. Zhou, Z.G. Huang, M.D. Wei, Sci. Res. 5 (2015) 11960.
[16] K.Q. Zhou, Z.S. Hong, C.B. Xie, H. Dai, Z.G. Huang, J. Alloys Comp. 651 (2015) 24–28.
[17] H. Geng, H. Ang, X. Ding, H. Tan, G. Guo, G. Qu, Y. Yang, J. Zheng, Q. Yan, H. Gu, Nanoscale 8 (2016) 2967–2973.
[18] Y. Zhong, X. Xia, J. Zhan, Y. Wang, X. Wang, J. Tu, J. Mater. Chem. A 4 (2016) 18717–18722.
[19] Z.S. Wu, G. Zhou, L.C. Yin, W. Ren, F. Li, H.M. Cheng, Nano Energy 1 (2012) 107–131.
[20] K. Lu, D. Li, X. Gao, H.X. Dai, N. Wang, H.Y. Ma, J. Mater. Chem. A 3 (2015) 16013.
[21] X. Tong, X. Xia, C. Guo, Y. Zhang, J. Tu, H.J. Fan, X.-Y. Guo, J. Mater. Chem. A 3 (2015) 18372–18379.
[22] X. Xia, D. Chao, Y. Zhang, J. Zhan, Y. Zhong, X. Wang, Y. Wang, Z.X. Shen, J. Tu, H. J. Fan, Small 12 (2016) 3048–3058.
[23] X. Xia, J. Zhan, Y. Zhong, X. Wang, J. Tu, H.J. Fan, Small (2016), http://dx.doi.org/10.1002/smll.201602742.
[24] W. Xia, A. Mahmood, R.Q. Zou, Q. Xu, Energy Environ. Sci. 8 (2015) 1837–1866.
[25] F. Shi, D. Xie, Y. Zhong, D.H. Wang, X.H. Xia, C.D. Gu, X.L. Wang, J.P. Tu, J. Power Sources 327 (2016) 281–288.
[26] F. Zou, Y.M. Chen, K.W. Liu, Z.T. Yu, W.F. Liang, S.M. Bhaway, M. Gao, Y. Zhu, ACS Nano 10 (2016) 377–386.
[27] L. Hu, Y. Huang, F. Zhang, Q. Chen, Nanoscale 5 (2013) 4186–4190.
[28] S.J. Yang, S. Nam, T. Kim, J.H. Im, H. Jung, J.H. Kang, S. Wi, B. Park, C.R. Park, J. Am. Chem. Soc. 135 (2013) 7394–7397.
[29] J. Shao, Z.M. Wan, H.M. Liu, H.Y. Zheng, T. Gao, M. Shen, Q.T. Qu, H.H. Zheng, J. Mater. Chem. A 2 (2014) 12194–12200.
[30] X.Y. Yu, L. Yu, H.B. Wu, X.W. Lou, Angew. Chem. 127 (2015) 5421–5425.
[31] G. Zhang, S. Hou, H. Zhang, W. Zeng, F. Yan, C.C. Li, H. Duan, Adv. Mater. 27 (2015) 2400–2405.

[32] R. Wu, D.P. Wang, X. Rui, B. Liu, K. Zhou, A.W. Law, Q. Yan, J. Wei, Z. Chen, Adv. Mater. 27 (2015) 3038–3044.
[33] P. Wang, J. Lang, D. Liu, X. Yan, Chem. Commun. 51 (2015) 11370–11373.
[34] J.F. Qian, F.A. Sun, L.Z. Qin, Mater. Lett. 82 (2012) 220–223.
[35] H. Hu, L. Han, M.Z. Yu, Z.Y. Wang, X.W. (David) Lou, Energy Environ. Sci. 9 (2015) 107–111.
[36] W. Huang, Z. Zuo, P. Han, Z. Li, T. Zhao, J. Electron. Spectrosc. 173 (2009) 88–95.
[37] R. Poulomi, S. Suneel Kumar, J. Mater. Chem. A 3 (2015) 2454.
[38] M. Hassan, M. Rahman, Z. Guo, Z. Chen, H. Liu, J. Mater. Chem. 20 (2010) 9707.
[39] H.G. Wang, Z. Wu, F.L. Meng, D.L. Ma, X.L. Huang, L.M. Wang, X.B. Zhang, ChemSusChem 6 (2013) 56–60.
[40] P. Poizot, S. Laruelle, S. Grugeon, L. Dupont, J.M. Tarascon, Nature 407 (2000) 496–499.
[41] S. Grugeon, S. Laruelle, L. Dupont, J.M. Tarascon, Solid State Sci. 5 (2003) 895–904.
[42] M. Dollé, P. Poizot, L. Dupont, J.M. Tarascon, Electrochem. Solid State Lett. 5 (2002) A18–A21.
[43] X. Xing, R.L. Liu, S.Q. Liu, Suo Xiao, Yi Xu, C. Wang, D.Q. Wu, Electrochim. Acta 194 (2016) 310–316.
[44] H.H. Li, Z.Y. Li, X.L. Wu, L.L. Zhang, C.Y. Fan, H.F. Wang, X.Y. Li, K. Wang, H.Z. Sun, J.P. Zhang, J. Mater. Chem. A 4 (2016) 8242.
[45] G.Q. Zou, J. Chen, Y. Zhang, C. Wang, Z.D. Huang, S.M. Li, H.X. Liao, J.F. Wang, X. B. Ji, J. Power Sources 325 (2016) 25–34.